Article

A Micro-hotplate-based Oven-controlled System used to Improve the Frequency Stability of MEMS Resonators

Tianren Feng [1,*], Duli Yu [1], Bo Wu [2] and Hui Wang [2]

[1] College of Information Science and Technology, Beijing University of Chemical Technology, Beijing 100029, China
[2] Guangdong Institute of Semiconductor Micro-nano Manufacturing Technology, Guangdong 528225, China
* Correspondence: trfeng@mail.buct.edu.cn (T.F.)

Abstract: This paper introduces a chip-level oven-controlled system for improving the temperature stability of MEMS resonators. Wherein the resonator and the micro-hotplate are manufactured by MEMS technology, then wire-bounded in a package shell at the chip level. The proposed resonator is transduced by the AlN film, and its temperature is monitored by temperature-sensing resistors on both sides. The designed micro-hotplate is placed at the bottom of the resonator chip as a heater and insulated by airgel. The PID pulse width modulation (PWM) circuit controls the heater according to the temperature detection result to provide a constant temperature for the resonator. The proposed oven-controlled MEMS resonator (OCMR) exhibits a frequency drift of 3.5ppm in the range of -50°C to 125°C, and the method also can be applied to other MEMS devices that require temperature control.

Keywords: resonators; OCMR; hotplate; temperature control; MEMS devices

1. Introduction

Temperature stability is critical for microelectromechanical systems (MEMS) device applications such as inertial sensing and frequency reference [1]. Silicon-based piezoelectric resonators are one of the most reported and used MEMS devices, and they have shown great potential to replace traditional quartz resonators in recent years [2]. However, the -30ppm/°C temperature coefficient (TCF) of MEMS resonators hinders their further development [3]. Uncompensated silicon MEMS resonators can cause problems such as clock drift, signal errors, loss of lock and etc. Therefore, it is very important to improve the temperature stability of MEMS resonators. Although some passive compensation methods such as heavily doped silicon or composite materials have been studied [4–6], it is difficult to obtain the highest temperature stability. Studies have shown that oven-controlled methods can achieve the highest frequency stability over the entire industrial temperature range [2–4,7–9]. For example, Xu designed a piezoelectric MEMS resonator with an integrated heater and achieved stability of 100 ppm from -35°C to 85°C [10]. Liu proposed an oven-controlled MEMS resonator (OCMR) using structural resistance as a temperature sensor, which achieved stability of ±0.3 ppm over the temperature range of -25 °C to 85 °C [3]. Jia proposed to simultaneously excite two modes on a resonator, and use the frequency shift of one of the modes as a temperature detection method. Low power consumption is achieved with the help of folded beams and an isolation frame, and stability of ±0.4ppm is achieved over the temperature range of −40 °C to 80 °C [2]. The above work proves that oven control technology is an effective method to improve the stability of MEMS devices by maintaining a constant temperature in real time [11]. However, almost all the reported oven control systems need to redesign the resonator structure or even change the process flow to meet the temperature control requirements, which will undoubtedly increase the risk of performance deterioration, yield decline, and cost increase of the resonator, thus hindering the commercialization process. At the same time, most OCMRs are designed for the traditional industrial temperature range of 85°C. With the continuous development of applications such as smart cars and the Internet of

Preprints (www.preprints.org) | NOT PEER-REVIEWED | Posted: 1 June 2023 doi:10.20944/preprints202306.0072.v1

Things (IoT), it is necessary to design OCMRs that meet a wide operating temperature range of 125°C to adapt to more fields.

Therefore, this paper proposes a chip-level oven-controlled system based on a micro-hotplate to improve the temperature stability of MEMS resonators in the range of -50°C to 125°C. First, the designed annular An-on-Si resonator and micro-hotplate are introduced. Secondly, the structure and control method of the oven-controlled system is described. Finally, the test results are discussed. Compared with other ovalized MEMS resonators, our work does not need to redesign or increase constraints on the MEMS resonator. It is applicable to a variety of MEMS devices, thus providing an ovalized solution for existing MEMS devices.

2. Devices design

In this work, we designed a piezoelectric MEMS resonator with a temperature measuring resistor and a micro-hotplate with a heating resistor, respectively. They are integrated in the same package through wire-boding to form an oven-controlled MEMS resonator. The sensing resistor is used to determine the temperature of the resonator and provide an input signal for the control loop, and the heating resistor is driven by the controller output signal to provide a constant temperature for the resonator chip, thereby improving its temperature stability.

2.1. MEMS resonator

The introduced piezoelectric MEMS resonator is designed based on AlN thin films on silicon-on-insulator (SOI) [12,13]. Figure 1 is the cross-sectional view of the piezoelectric resonator designed in this paper. The substrate silicon is used to support the entire device structure, the top silicon is the main body of the resonator, and the three layers above the top silicon are the isolation layer (AlN), the bottom electrode (Mo), the piezoelectric layer (AlN) and the top electrode (Mo). The top electrode port is used to connect external input or output signals, and form an electric field with the grounded bottom electrode. The resonator suspends the structure by releasing the oxide sacrificial layer to achieve free vibration. When the AC signal is input at the signal port, the electric field will be generated between the input and the bottom electrode. According to the inverse piezoelectric effect, the piezoelectric film will generate lateral stretching stress, and the resonator will also vibrate laterally. When the excitation frequency is close to the nature frequency, the structure will resonate, and the deformation law in this state is called the resonant mode. At the same time, the piezoelectric layer will also be deformed due to the vibration of the resonator, so that a moving charge will be generated in the piezoelectric film, and the charge can be collected at the output electrode to form a current output, and the output signal is amplified to measure the resonance frequency. Figure 2a shows the realization of the designed ring resonator in this paper, the electric field applied across the thickness of the resonator tends to expand the structure and cause it to resonate in breathing mode [14]. For the ring resonator, the first in-plane breathing mode resonance frequency can be calculated using [15]:

$$f_0 = (1/2\pi)\sqrt{E_Y / (\rho R_1 R_2)} \quad (1)$$

where E_Y is the Young's modulus, ρ is the density. R_1 is designed to have an inner diameter of 200um, and R_2 is designed to have an outer diameter of 400um. The frequency is approximately equal to 5.7Mhz. The equivalent Young's modulus and equivalent density are calculated based on the average value of AlN and Si thickness proportions, and the modal also can be calculated based on COMSOL finite element simulation.

The main materials of the resonator are AlN and Si respectively. Table 1 shows its material constants [15]. Since the mode is insensitive to device thickness variations, adding an additional thin layer does not significantly change the resonant frequency of this mode.

Preprints (www.preprints.org) | NOT PEER-REVIEWED | Posted: 1 June 2023 doi:10.20944/preprints202306.0072.v1

Table 1. Material constants used in simulations.

Parameter	Si	AlN
Young's modulus (GPa)	170	345
Mass density (kg·m^{-3})	2329	3300
Thermal expansion coefficient (K^{-1})	2.6×10^{-6}	4.2×10^{-6}
Thermal conductivity (W·m^{-1}·K^{-1})	130	60
Heat capacity (J·kg^{-1}·K^{-1})	700	600

As shown in Figure 2b, the serpentine sensing resistor is placed near the resonant structure, defined at the same time as the top electrode of the resonator, so it can be realized without modifying the existing manufacturing process of the resonator. It is well known that metal resistance can be used as a temperature sensor due to the temperature dependence [16].

Figure 3 shows the process flow. First, a layer of 50 nm thick AlN is grown on the 2um thick top silicon layer as a seed layer, and then 0.2/1/0.2um thick Mo/AlN/Mo are respectively deposited as the bottom electrode, piezoelectric layer and top electrode. Then a series of etching processes are used to define the shape of the electrode and the resonator respectively, and finally the buried oxide layer is removed to release the device. Figure 2c shows the microscope image of the ring resonator. It can be seen from the figure that the ring resonator is anchored on the substrate by four supporting beams and fully released, and the electrodes for frequency and sensing signals are all brought to the edge of the chip for wire-bonding.

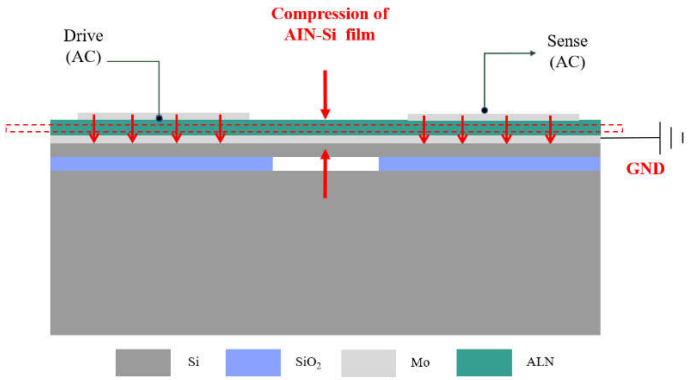

Figure 1. Cross-sectional view of the resonator.

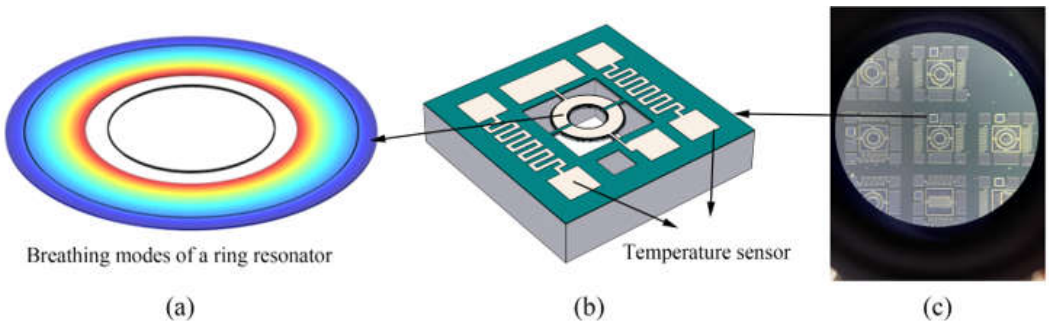

Figure 2. (a)Simulation results showing mode shape; (b)schematic of the ring resonator chip; (c) The microscope image of the ring resonator.

Preprints (www.preprints.org) | NOT PEER-REVIEWED | Posted: 1 June 2023 doi:10.20944/preprints202306.0072.v1

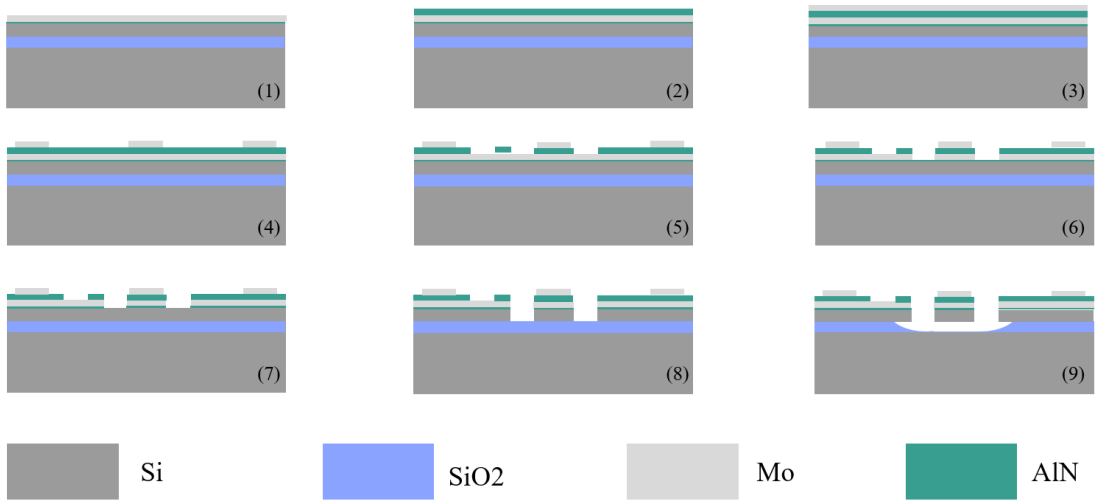

Figure 3. The process flow used to fabricate resonators.

2.2. Micro hotplate

Micro-hotplates have attracted the attention of gas sensor researchers due to their advantages of fast response, uniform temperature distribution, and low power consumption [17]. The existing micro-hotplates can be divided into closed-film structure and suspended-film structure according to structure classification [17,18]. However, the micro-hotplates of both structures have relatively high film stress, so the core area is often unable to bear the weight [19,20]. In addition, the suspended micro-hotplate also requires additional deep reactive ion etching (DRIE), which will additionally increase the manufacturing cost [21]. In this paper, the airgel film is placed at the bottom of the micro-hot plate instead of the suspended heat insulation structure, so the overall structure can be guaranteed to be stable. As shown in Figure 4, the silicon substrate is used as the main body of the micro-hotplate, and the silicon is separated by an isolation layer (SiO2) and an electrode (Al). By applying DC voltage to the ports on both sides of the electrode, the temperature of the micro-hot plate is increased by means of electrocaloric effect. Figure 5a shows the thermal distribution of the micro-hotplate designed in this paper, and the electrode shape with the most uniform temperature distribution was determined through COMSOL finite element simulation [22–24]. The simulation results show that the temperature of the micro-hotplate can be increased rapidly and its temperature distribution is less than 1.5°C by adding a DC voltage to both ends of the serpentine electrode. Figure 5b shows a schematic diagram of the micro-hotplate chip, and 200um thick commercial SiO2 airgel was pasted on the bottom of the micro-hotplate to enhance thermal insulation. The size of the micro-hotplate is 6 mm × 6 mm, the electrode width and spacing are 180 um, and the serpentine electrode shape ensures the temperature uniformity in the heating area [25]. Figure 6 shows the process flow. First, a 525um thick silicon substrate ensures the consistency with the thermal expansion of the resonator chip, then a 300nm thick oxide layer is grown for electrical isolation, and then a 300nm thick Al metal layer is deposited. Finally, the electrode shape is defined by an etching process. Figure 5c shows a micrograph of the micro-hotplate chip.

During the design process of the micro-hotplate, its heat transfer characteristics need to be considered to ensure that it can provide sufficient heating effect. There are three main ways of heat dissipation in the micro-hot plate [26], namely heat conduction, heat convection, and heat radiation, among which the heat loss caused by heat conduction is the main way [21,27]. The different components of heat loss can be expressed as:

$$Q_{tot} = G_m \lambda_m \left(T_{hot} - T_{amb}\right) + G_{air} \lambda_{air} \left(T_{hot} - T_{amb}\right) + G_{rad} \sigma \varepsilon \left(T_{hot}^4 - T_{amb}^4\right) \quad (2)$$

where G_m, G_{air}, and G_{rad} are geometric factors, mainly determined by structural design. T_{hot} and T_{amb} are the temperature of the active area and the ambient temperature, respectively. λ_m and λ_{air}

Preprints (www.preprints.org) | NOT PEER-REVIEWED | Posted: 1 June 2023 doi:10.20944/preprints202306.0072.v1

are the thermal conductivity of the micro-hotplate and the surrounding atmosphere, ε is the emissivity, and σ is the Boltzmann constant [21].

G_m is the structural geometric factor, which is proportional to the area of the heat transfer path and inversely proportional to the length of the heat transfer path. λ_m is the coefficient of heat conduction, the 200um thick airgel increases the heat transfer path, and its heat transfer coefficient is about 0.02W/m²·K, which is much smaller than the heat transfer coefficient of the silicon substrate, so it can be very effective in heat insulation. At the same time, the designed micro-hotplate has high mechanical strength, and the residual stress and thermal stress can be well controlled. When the micro-hot plate is directly exposed to the gas environment and there is a significant temperature difference from the ambient temperature, the convection coefficient is required when calculating the heat dissipation caused by natural convection. Generally, the convection coefficient in natural air can be taken as 5W/(m²·K). If the micro-hotplate is vacuum-sealed so that the internal pressure is at the millitorr level, gas convection and conduction can be neglected. For thermal radiation, according to the Stefan-Boltzmann law, the thermal radiation flux of a small-volume MEMS device can be simply expressed as:

$$Q = \frac{4\pi\lambda_{air}\left(T_{hot} - T_{amb}\right)}{1/r_i - 1/r_a} \approx 4\pi r_i \lambda_{air}\left(T_{hot} - T_{amb}\right) \quad (3)$$

where r_i and r_a are the effective radii of the heating zone and the device as a whole, respectively.

Generally, the thermal radiation power consumption of MEMS devices can usually be ignored. Therefore, this paper mainly uses airgel to reduce heat conduction. After considering all the heat dissipation paths mentioned above, the simulation verifies the heating function of the micro-hotplate. As shown in Figure 5a, when 1.5W is applied to the heater, the temperature can be raised to 135°C. Considering that the equivalent resistance of the designed Al heater is about 40Ω, a conventional power supply with a voltage of 12V and a current of 0.5A is sufficient to meet the requirements. Simulation results show that the thermal insulation performance is improved by tens of times compared with the case without airgel insulation. Although the power consumption of the proposed micro-hotplate is still higher than that of the suspended structure, sufficient mechanical stability is guaranteed. The proposed micro-hotplate thus achieves a good performance compromise and is a viable option for non-low-power applications.

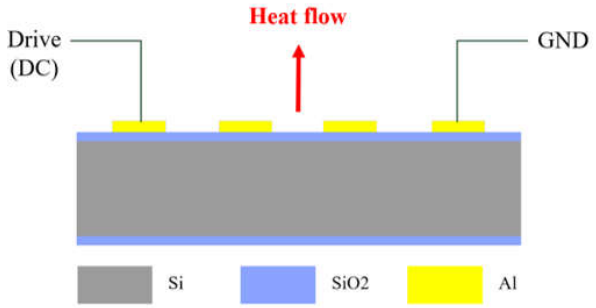

Figure 4. Cross-sectional view of the hotplate.

Preprints (www.preprints.org) | NOT PEER-REVIEWED | Posted: 1 June 2023 doi:10.20944/preprints202306.0072.v1

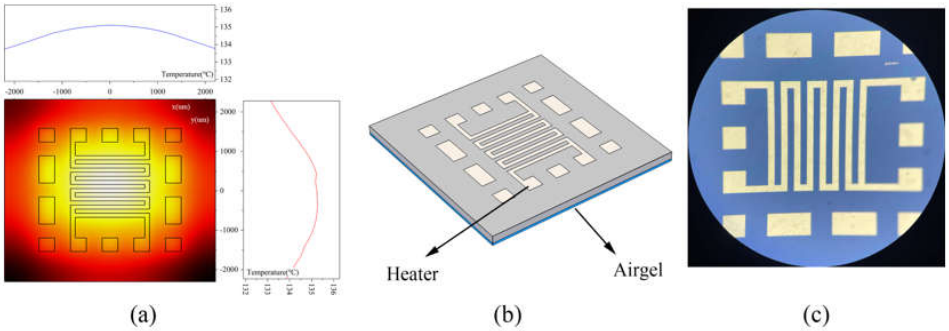

Figure 5. (a)Simulation results showing heat distribution; (b)schematic of the hotplate chip; (c) The microscope image of the hotplate.

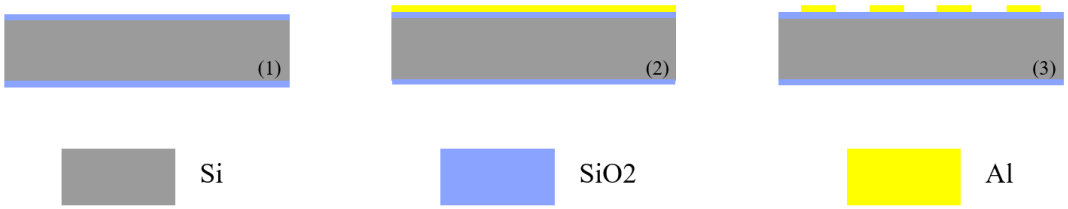

Figure 6. The process flow used to fabricate hotplate.

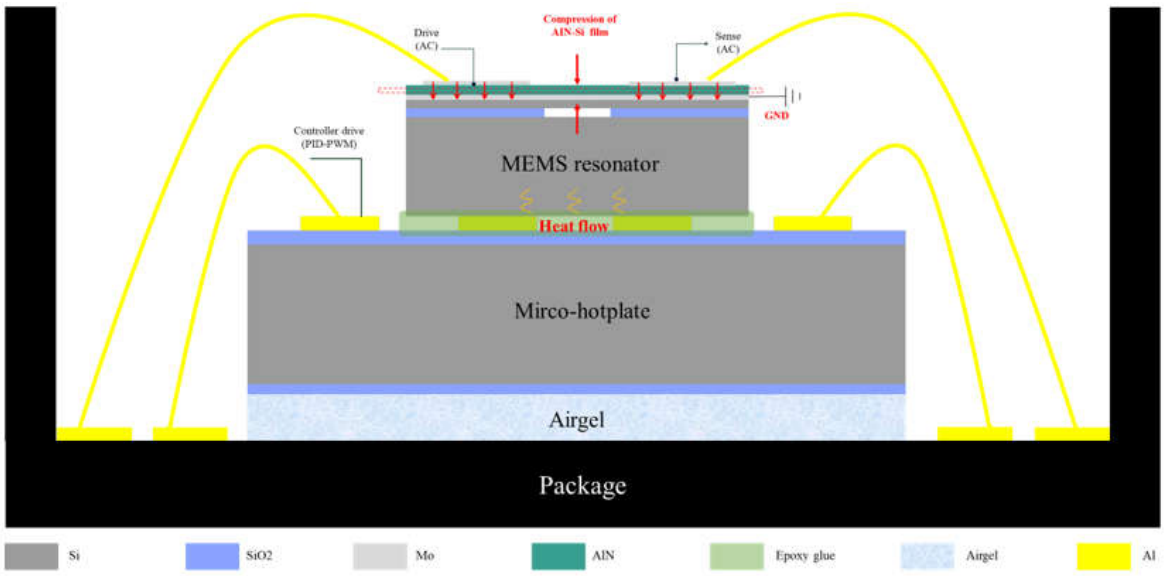

Figure 7. Cross-sectional view of the proposed oven-controlled system.

3. Oven-controlled system

In order to avoid the influence of ambient temperature on the MEMS resonator, an oven-controlled system based on a micro-hot plate is proposed. As shown in Figure 7, it is mainly composed of a resonator chip, a micro-hot plate chip and a package shell. They are fixed by epoxy resin [11], and a 200um thick SiO2 airgel film is placed between the micro-hotplate chip, and the bottom of the package to enhance thermal insulation. The resonator chip attached to the micro-hotplate can be heated to ensure that it operates at a relatively stable temperature [28]. The electrical contact is made by wire-bonding [29].

Preprints (www.preprints.org) | NOT PEER-REVIEWED | Posted: 1 June 2023 doi:10.20944/preprints202306.0072.v1

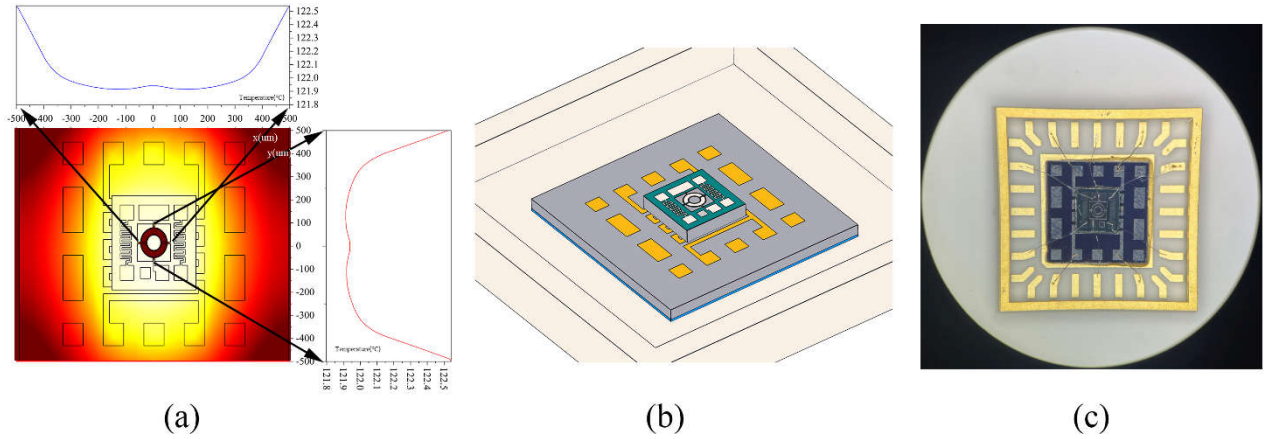

Figure 8. (a)Simulation results showing heat distribution; (b)schematic of the OCMR chip; (c) The microscope image of the OCMR.

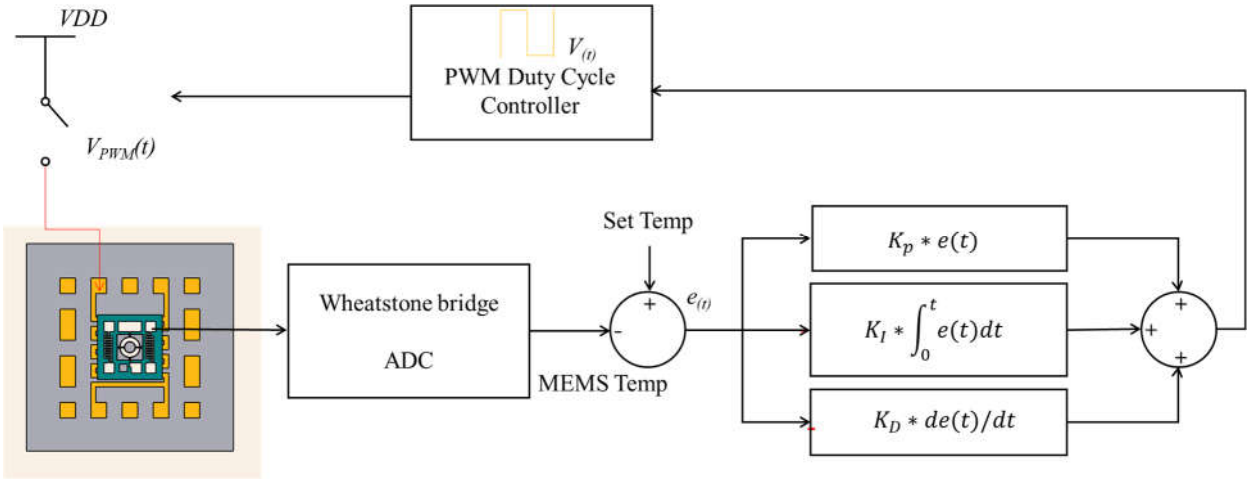

Figure 9. Block diagram of control principle.

The simulation results show that the micro-hotplate can heat the resonator chip. Figure 8a shows the thermal distribution of the designed OCRM. With the help of the uniform heating of the micro-hotplate and the high thermal conductivity of the silicon substrate, the temperature distribution on the resonator structure is less than 0.6 °C. Figure 8b and Figure 8c show the schematic structure and micrograph of OCMR, respectively. The resonator chip is placed in the center of the micro-hot plate, and the signal ports are connected to the pads of the package shell through gold wires, and then the whole system can be soldered on the PCB to realize an electrical connection with the control circuit. Figure 9 shows the control system principle. Thanks to the temperature-resistivity coefficient of metals with high linearity, when the external temperature changes, the change in resistance will be converted into a temperature signal through the bridge and ADC [11,30]. The controller will compare the error between the set temperature and the detected temperature [30], and then calculate the corresponding control signal through the PID algorithm and convert it into the duty cycle of pulse width modulation (PWM) [16]. Finally, the on-off condition of the MOS tube is controlled by changing the duty cycle to drive the heating resistor with an appropriate power to ensure a constant temperature of the MEMS resonator chip [31,32]. The functions of the control system are realized on the external PCB.

Preprints (www.preprints.org) | NOT PEER-REVIEWED | Posted: 1 June 2023 doi:10.20944/preprints202306.0072.v1

4. Experiments and Results

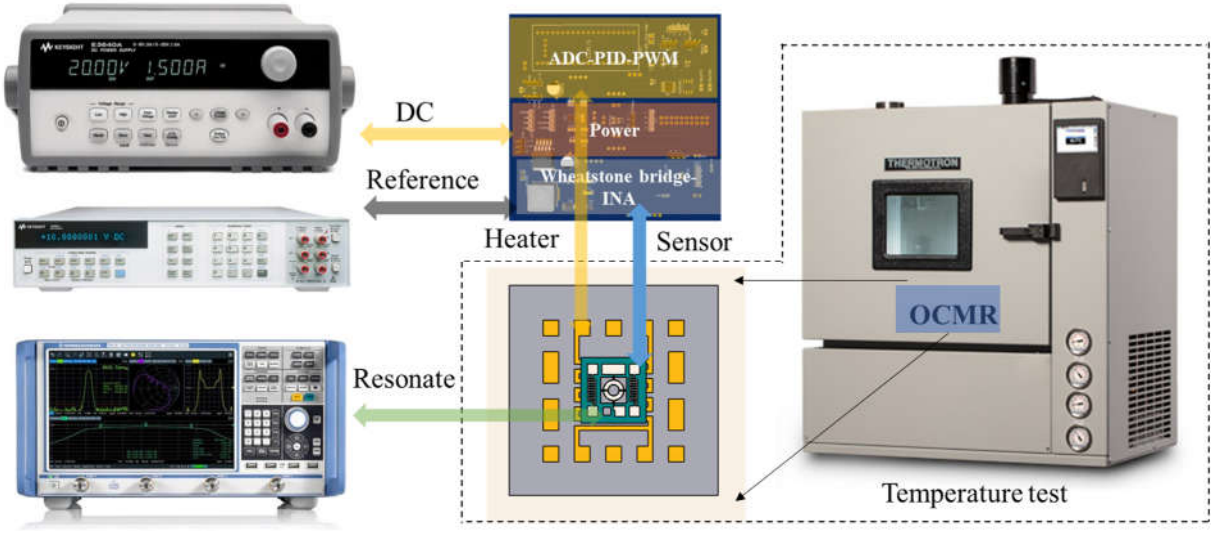

Figure 10. Experiment block diagram.

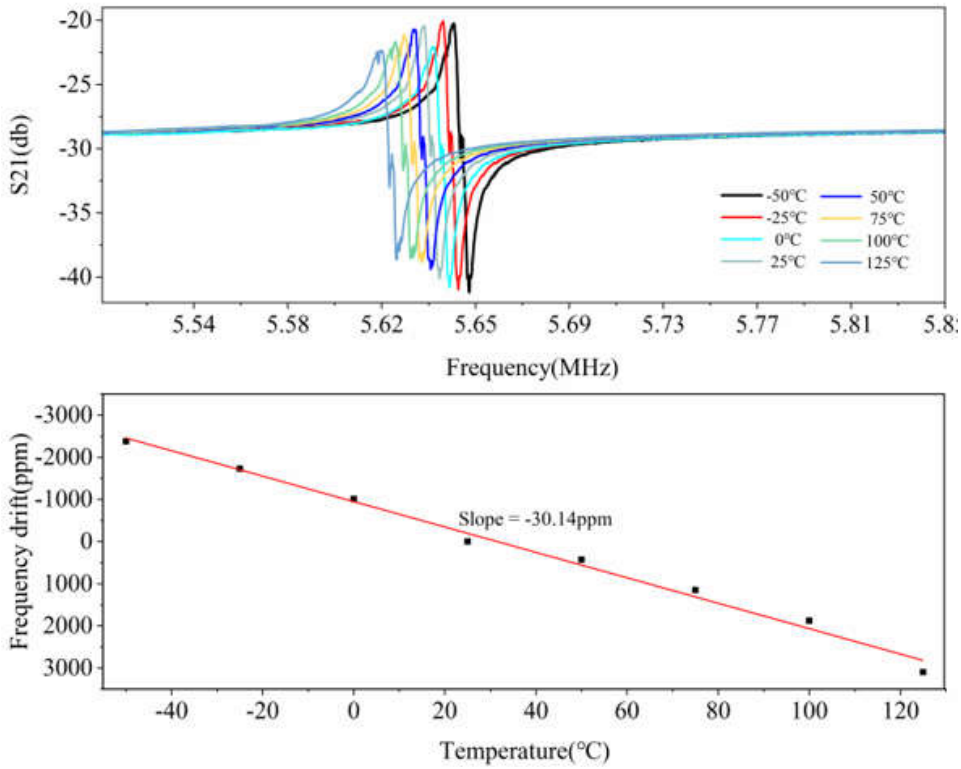

Figure 11. Temperature characteristic test results: resonance frequency shift.

The experimental block diagram is shown in Figure 10. The constant temperature MEMS resonator is placed in a high temperature box to verify the temperature characteristics of OCMR. Connect the input and output electrodes of the resonator to a network analyzer, read the S21 parameters, and verify the performance of the MEMS resonator.

The temperature of the high-temperature box is changed from -50°C to 125°C, each temperature point is separated by 25°C, and each temperature point lasts for 20 minutes to ensure that the temperature is stable. The resonant frequency at each temperature point are recorded and fitted to the test data points. Figure 11 shows the variation of the resonant frequency with temperature. The results show that the characteristic characteristics of the resonator is affected by the ambient

Preprints (www.preprints.org) | NOT PEER-REVIEWED | Posted: 1 June 2023 doi:10.20944/preprints202306.0072.v1

temperature to have a (TCF) temperature coefficient of -30.14 ppm/°C. At the same time, the resonant frequency of the designed MEMS piezoelectric resonator is 5.63MHz, and the slight difference with the simulation result can be explained as the influence of fabrication error. Its insertion loss is -20db and its quality factor is 1400. When the resonant frequency at 25°C is used as a reference, its maximum frequency drift in a wide temperature range reaches 3100ppm, so it must be temperature controlled to improve temperature stability.

The controller parameters are designed according to the test data. Experimental results show that in addition to PID coefficients, the PWM resolution and carrier frequency also have an impact on the control effect. As shown in Figure 12, the control effects under different PWM frequencies are compared. It can be observed that as the PWM frequency decreases, the system temperature vibrates obviously. Because low PWM frequency will cause the non-ideal characteristics of the equivalent voltage and deteriorate the control effect. When the PWM frequency is set to 100Hz, the maximum steady-state error exceeds 5°C, and when the PWM frequency is set to 10kHz, the stability can reach 0.5°C. As shown in Figure 13, as the duty cycle resolution decreases, the steady-state error of the system increases. When the duty cycle resolution is higher, the control effect is improved. Since the proposed constant temperature system itself has a thermal low-pass characteristic, the higher PWM frequency and resolution will not introduce additional harmonics to the system. A frequency of 1kHz and a duty cycle resolution of 0.01% was finally chosen. The test results show that the proposed OCMR can realize the temperature control function and has a temperature stability of 0.5 °C.

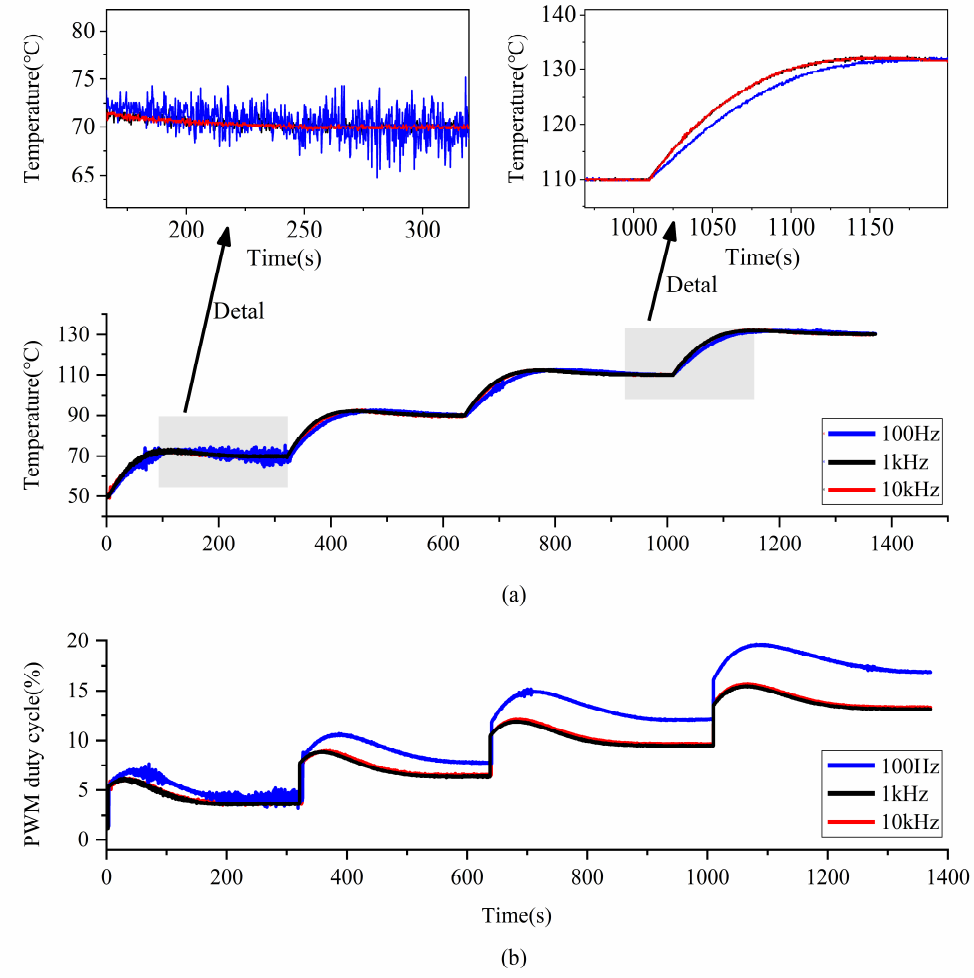

Figure 12. Under different PWM frequencies: (a) temperature control effect and details; (b) duty cycle.

Preprints (www.preprints.org) | NOT PEER-REVIEWED | Posted: 1 June 2023 doi:10.20944/preprints202306.0072.v1

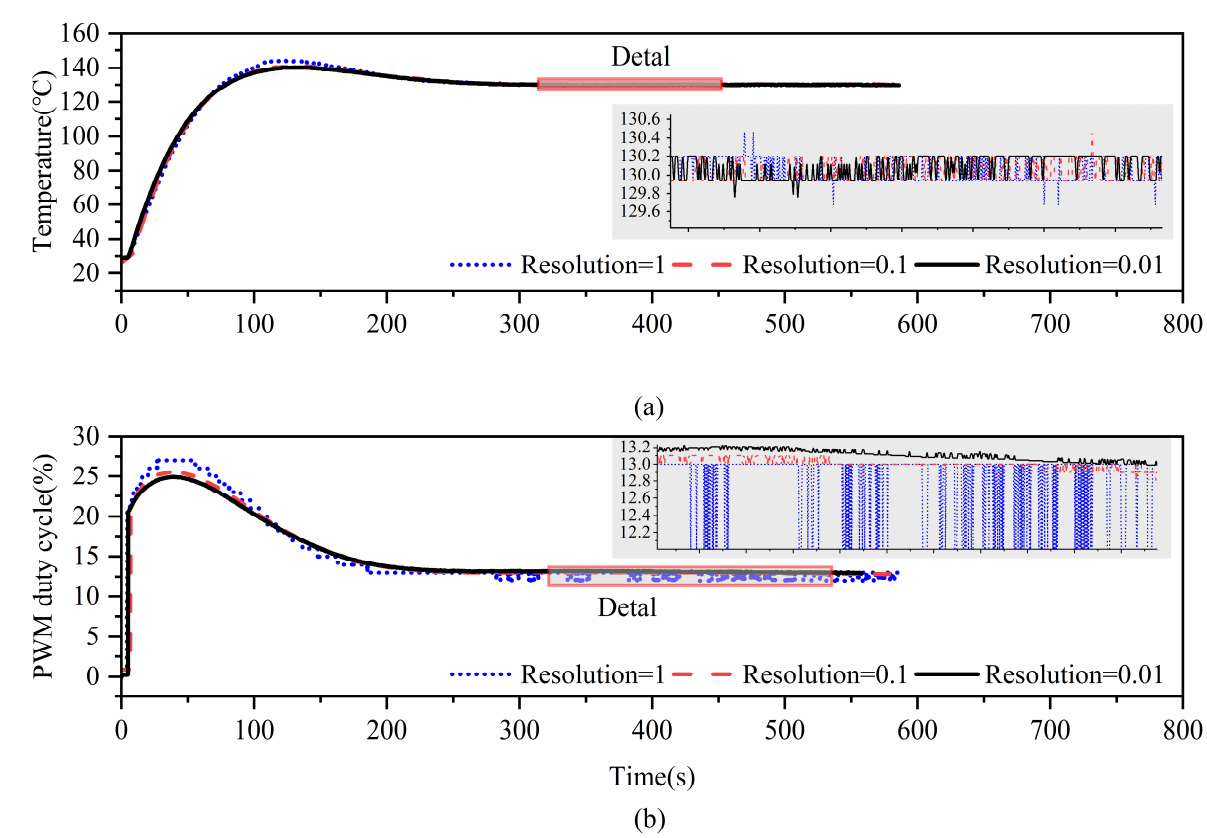

Figure 13. (a)Temperature control effect and details; (b) Output duty cycle under different PWM resolutions.

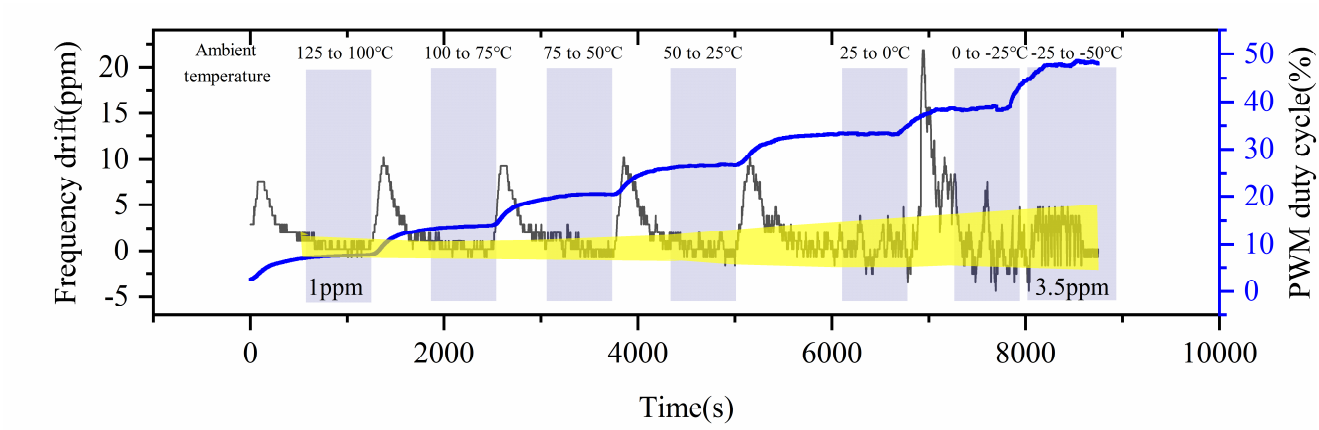

Figure 14. PWM temperature control duty cycle and resonator frequency shift under different external temperatures.

Figure 14 shows the frequency shift of the OCMR when the external temperature decreases from 125°C to -50°C. In order to meet the operating temperature range of 125°C, the control system keeps the temperature of the MEMS resonator constant at 130°C. It should be noted that since the test process is uninterrupted, the dynamic process needs to be ignored when discussing temperature stability, and the results of the steady-state process are highlighted in the figure. The results show that the OCMR has a maximum frequency drift of 3.5 ppm and a nearly thousand-fold improvement in temperature stability compared to a MEMS resonator without temperature control, thus demonstrating the effectiveness of the proposed method. The frequency drift of OCMR is only 1ppm around 125°C. However, as the ambient temperature decreases, the PWM output power increases, and the temperature offset of OCMR changes from 1ppm to 3.5ppm. This may be because when the

 doi:10.20944/preprints202306.0072.v1

temperature difference between the resonator and the outside temperature is too large, the high heater power causes its resistance to change, thus deteriorating the control effect.

5. Conclusion

For MEMS resonator applications, temperature drift is still the most important problem to be solved. This paper demonstrates a MEMS resonator constant temperature system based on a micro-hot plate, which relies on the sensing resistor on the MEMS resonator chip to monitor the temperature in real-time and controls it through the heating resistor on the micro-hot plate. It has the advantages of strong versatility and easy implementation, achieving a stability of 3.5 ppm in the temperature range of -50°C to 125°C. In addition, the method proposed in this paper does not need to modify the design of the resonator, so it can be applied to other MEMS devices that require temperature control. In future work, the power consumption will be reduced by optimizing the thermodynamic structure and vacuum packaging.

Author Contributions: Conceptualization, T.F. and D.Y.; methodology, T.F. and D.Y.; writing—original draft preparation, T.F.; writing—review and editing, D.Y.; visualization, T.F. and B.W.; supervision, B.W. and H.W. All authors have read and agreed to the published version of the manuscript.

Funding: This research was funded by the National Natural Science Foundation of China (61874116) and by Fundamental Research Funds for the Central Universities (buctrc 202139).

Data Availability Statement: Not applicable.

Conflicts of Interest: The authors declare no conflict of interest.

References

1. Wu, Z.; Rais-Zadeh, M. A Temperature-Stable Piezoelectric MEMS Oscillator Using a CMOS PLL Circuit for Temperature Sensing and Oven Control. *Journal of Microelectromechanical Systems* **2015**, *24*, 1747–1758, doi:10.1109/JMEMS.2015.2434832.

2. Jia, W.; Chen, W.; Xiao, Y.; Wu, Z.; Wu, G. A Micro-Oven-Controlled Dual-Mode Piezoelectric MEMS Resonator With ±400 PPB Stability Over −40 to 80 °C Temperature Range. *IEEE Transactions on Electron Devices* **2022**, *69*, 2597–2603, doi:10.1109/TED.2022.3159287.

3. C. -S. Liu; R. Tabrizian; F. Ayazi A ±0.3 Ppm Oven-Controlled MEMS Oscillator Using Structural Resistance-Based Temperature Sensing. *IEEE Transactions on Ultrasonics, Ferroelectrics, and Frequency Control* **2018**, *65*, 1492–1499, doi:10.1109/TUFFC.2018.2843781.

4. Kwon, H.-K.; Ortiz, L.C.; Vukasin, G.D.; Chen, Y.; Shin, D.D.; Kenny, T.W. An Oven-Controlled MEMS Oscillator (OCMO) With Sub 10mw, ± 1.5 PPB Stability Over Temperature. In Proceedings of the 2019 20th International Conference on Solid-State Sensors, Actuators and Microsystems & Eurosensors XXXIII (TRANSDUCERS & EUROSENSORS XXXIII); June 2019; pp. 2072–2075.

5. Ahmed, H.; Rajai, P.; Ahamed, M.J. Temperature Frequency Stability Study of Extensional Mode N-Doped Silicon MEMS Resonator. *AIP Advances* **2022**, *12*, 015319, doi:10.1063/5.0074694.

6. Schwartz, S.A.; Brand, O.; Beardslee, L.A. Temperature Compensation of Thermally Actuated, In-Plane Resonant Gas Sensor Using Embedded Oxide-Filled Trenches. *Journal of Microelectromechanical Systems* **2020**, *29*, 936–941, doi:10.1109/JMEMS.2020.3014502.

7. Comenencia Ortiz, L.; Kwon, H.-K.; Rodriguez, J.; Chen, Y.; Vukasin, G.D.; Heinz, D.B.; Shin, D.D.; Kenny, T.W. Low-Power Dual Mode MEMS Resonators With PPB Stability Over Temperature. *Journal of Microelectromechanical Systems* **2020**, *29*, 190–201, doi:10.1109/JMEMS.2020.2970609.

8. Wang, Y.; Cao, R.; Li, C.; Dean, R.N. Concepts, Roadmaps and Challenges of Ovenized MEMS Gyroscopes: A Review. *IEEE Sensors Journal* **2021**, *21*, 92–119, doi:10.1109/JSEN.2020.3012484.

9. You, W.; Pei, B.; Sun, K.; Zhang, L.; Yang, H.; Li, X. Oven Controlled N++ [1 0 0] Length-Extensional Mode Silicon Resonator with Frequency Stability of 1 Ppm over Industrial Temperature Range. *J. Micromech. Microeng.* **2017**, *27*, 095002, doi:10.1088/1361-6439/aa7d1c.

10. Xu, C.; Segovia-Fernandez, J.; Kim, H.J.; Piazza, G. Temperature-Stable Piezoelectric MEMS Resonators Using Integrated Ovens and Simple Resistive Feedback Circuits. *Journal of Microelectromechanical Systems* **2017**, *26*, 187–195, doi:10.1109/JMEMS.2016.2626920.

11. Liu, Z.; Du, L.; Zhao, Z.; Liu, J.; Wu, P.; Fang, Z. A Chip-Level Oven-Controlled System Used to Improve Accuracy of Silicon Piezoresistive Pressure Sensor. *Measurement* **2019**, *143*, 1–10, doi:10.1016/j.measurement.2019.05.014.

12. Chen, W.; Jia, W.; Xiao, Y.; Feng, Z.; Wu, G. A Temperature-Stable and Low Impedance Piezoelectric MEMS Resonator for Drop-in Replacement of Quartz Crystals. *IEEE Electron Device Letters* **2021**, *42*, 1382–1385, doi:10.1109/LED.2021.3094319.

13. Wu, G.; Xu, J.; Zhang, X.; Wang, N.; Yan, D.; Lim, J.L.K.; Zhu, Y.; Li, W.; Gu, Y. Wafer-Level Vacuum-Packaged High-Performance AlN-on-SOI Piezoelectric Resonator for Sub-100-MHz Oscillator Applications. *IEEE Transactions on Industrial Electronics* **2018**, *65*, 3576–3584, doi:10.1109/TIE.2017.2748041.

14. Piazza, G.; Stephanou, P.J.; Pisano, A.P. Piezoelectric Aluminum Nitride Vibrating Contour-Mode MEMS Resonators. *Journal of Microelectromechanical Systems* **2006**, *15*, 1406–1418, doi:10.1109/JMEMS.2006.886012.

15. Peczalski, A.; Zheng, X.-Q.; Lee, J.; Feng, P.X.-L.; Rais-Zadeh, M. Effects of Heterostructure Stacking on Acoustic Dissipation in Coupled-Ring Resonators. In Proceedings of the 2017 IEEE 30th International Conference on Micro Electro Mechanical Systems (MEMS); January 2017; pp. 954–957.

16. Zhang, M.; Zhao, Z.; Du, L.; Fang, Z. A Film Bulk Acoustic Resonator-Based High-Performance Pressure Sensor Integrated with Temperature Control System. *J. Micromech. Microeng.* **2017**, *27*, 045004, doi:10.1088/1361-6439/aa5e6a.

17. Yuan, Z.; Yang, F.; Meng, F. Research Progress on Coating of Sensitive Materials for Micro-Hotplate Gas Sensor. *Micromachines* **2022**, *13*, 491, doi:10.3390/mi13030491.

18. Liu, Q.; Yao, J.; Wu, Y.; Wang, Y.; Ding, G. Two Operating Modes of Palladium Film Hydrogen Sensor Based on Suspended Micro Hotplate. *International Journal of Hydrogen Energy* **2019**, *44*, 11259–11265, doi:10.1016/j.ijhydene.2019.02.228.

19. Xu, L.; Li, T.; Gao, X.; Wang, Y. Development of a Reliable Micro-Hotplate With Low Power Consumption. *IEEE Sensors Journal* **2011**, *11*, 913–919, doi:10.1109/JSEN.2010.2064765.

20. Liu, Q.; Wang, Y.; Yao, J.; Ding, G. Impact Resistance and Static Strength Analysis of an Extremely Simplified Micro Hotplate with Novel Suspended Film. *Sensors and Actuators A: Physical* **2018**, *280*, 495–504, doi:10.1016/j.sna.2018.08.003.

21. Prasad, M.; Dutta, P.S. Development of Micro-Hotplate and Its Reliability for Gas Sensing Applications. *Appl. Phys. A* **2018**, *124*, 788, doi:10.1007/s00339-018-2210-4.

22. Joy, S.; Antony, J.K. Design and Simulation of a Micro Hotplate Using COMSOL Multiphysics for MEMS Based Gas Sensor. In Proceedings of the 2015 Fifth International Conference on Advances in Computing and Communications (ICACC); September 2015; pp. 465–468.

23. Kumar, H.; Singh, K.K.; Sood, N.; Kumar, A.; Mittal, R.K. Design and Simulation of a Micro Hotplate for MEMS Based Integrated Gas Sensing System. In Proceedings of the 2014 IEEE Sensors Applications Symposium (SAS); February 2014; pp. 181–184.

24. Sidek, O.; Ishak, M.Z.; Khalid, M.A.; Abu Bakar, M.Z.; Miskam, M.A. Effect of Heater Geometry on the High Temperature Distribution on a MEMS Micro-Hotplate. In Proceedings of the 2011 3rd Asia Symposium on Quality Electronic Design (ASQED); July 2011; pp. 100–104.

25. Kharbanda, D.K.; Suri, N.; Khanna, P.K. Design, Fabrication and Characterization of Laser Patterned LTCC Micro Hotplate with Stable Interconnects for Gas Sensor Platform. *Microsyst Technol* **2019**, *25*, 2197–2204, doi:10.1007/s00542-018-4079-8.

26. Li, D.; Ruan, Y.; Chen, C.; He, W.; Chi, C.; Lin, Q. Design and Thermal Analysis of Flexible Microheaters. *Micromachines* **2022**, *13*, 1037, doi:10.3390/mi13071037.

27. Zhao, W.-J.; Xu, D.; Chen, Y.-S.; Wang, X.; Shi, Y.-B. A Low-Temperature Micro Hotplate Gas Sensor Based on AlN Ceramic for Effective Detection of Low Concentration NO2. *Sensors* **2019**, *19*, 3719, doi:10.3390/s19173719.

28. Zhang, Y.; Hao, X.; Huang, W.; Zhang, W.; Wang, J. Active and Accurate Temperature Control of Terahertz Functional Devices Using a Micro-Hotplate System. *J. Phys. D: Appl. Phys.* **2021**, *55*, 135108, doi:10.1088/1361-6463/ac42fa.

29. Chen, J.; Lu, Q.; Bai, J.; Xu, X.; Yao, Y.; Fang, W. A Temperature Control Method for Microaccelerometer Chips Based on Genetic Algorithm and Fuzzy PID Control. *Micromachines* **2021**, *12*, 1511, doi:10.3390/mi12121511.

30. Jeroish, Z.E.; Bhuvaneshwari, K.S.; Samsuri, F.; Narayanamurthy, V. Microheater: Material, Design, Fabrication, Temperature Control, and Applications—a Role in COVID-19. *Biomed Microdevices* **2021**, *24*, 3, doi:10.1007/s10544-021-00595-8.

31. Nordin, A.N.; Voiculescu, I.; Zaghloul, M. Micro-Hotplate Based Temperature Stabilization System for CMOS SAW Resonators. *Microsyst Technol* **2009**, *15*, 1187–1193, doi:10.1007/s00542-009-0786-5.

32. Lahijani, B.V.; Badri Ghavifekr, H. Design of a SAW-Based Sensor Combined with a Micro-Hotplate for Biological Applications. In Proceedings of the 2010 17th Iranian Conference of Biomedical Engineering (ICBME); November 2010; pp. 1–4.